Colloids and Surfaces A: Physicochemical and Engineering Aspects 673 (2023) 131799

Contents lists available at ScienceDirect

Colloids and Surfaces A: Physicochemical and Engineering Aspects

journal homepage: www.elsevier.com/locate/colsurfa

Physico-chemical characterization of Synperonic™ 91/5 self-assembly behaviour in water

Sara Falsini [a], Adriano Intiso [b], Francesco Spinozzi [c], Sandra Ristori [d,*], Nadia Marchettini [e], Javier I. Garza-Arévalo [f], Sylvain Prevost [g], Margarita Sanchez-Dominguez [f,*], Federico Rossi [e,*]

[a] Department of Biology, University of Firenze, via Micheli 1, 50121 Florence, Italy
[b] Department of Chemistry and Biology "A. Zambelli", University of Salerno, Via Giovanni Paolo II 132, 84084 Fisciano, SA, Italy
[c] Dipartimento di Scienze della Vita e dell'Ambiente, Università Politecnica di Ancona, Via delle Brecce Bianche, 60131 Ancona, Italy
[d] Department of Chemistry "Ugo Schiff" & CSGI, University of Firenze, Via della Latruccia 3, 50019 Sesto Fiorentino, FI, Italy
[e] Department of Earth, Environmental and Physical Sciences "DEEP Sciences", University of Siena, Pian dei Mantellini 44, 53100 Siena, Italy
[f] Grupo de Química Coloidal e Interfacial Aplicada a Nanomateriales y Formulaciones, Centro de Investigación en Materiales Avanzados, S.C. (CIMAV), Unidad Monterrey, Alianza Norte 202, Parque de Investigación e Innovación Tecnológica, 66628 Apodaca, Nuevo León, Mexico
[g] Large Scale Structures, Institut Laue-Langevin, 71 avenue des Martyrs, CS 20156, 38042 Grenoble Cedex 9, France

GRAPHICAL ABSTRACT

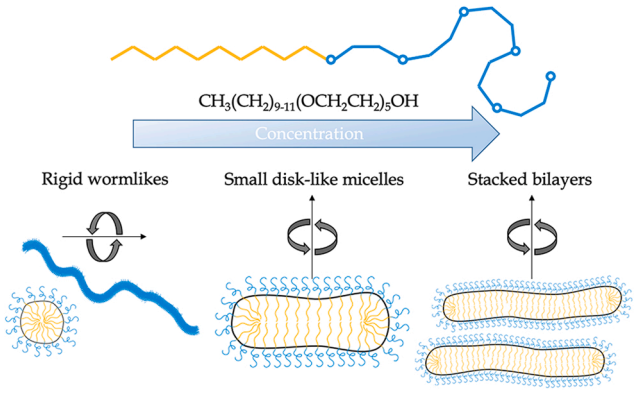

ARTICLE INFO

Keywords:
Synperonic
SAXS
SANS
Micelles, Surfactant
Ethoxylated fatty alcohols
Scattering

ABSTRACT

We studied the self-assembled aggregates of Synperonic™ 91/5 (SYN) in water solution. This surfactant presents the peculiarity of having an odd number of aliphatic carbons, with a tail composed of C_9H_{19} and $C_{11}H_{23}$, and the headgroup having an average of 5 ethoxy units. While the general family of C_iEO_j nonionic surfactants has been widely studied, there is little knowledge for the case of surfactants with odd-number carbons. For this reason, we carried out an in depth physico-chemical characterization of water solutions containing SYN in the wide range of concentration from 2 % to 50 % (i.e. 0.05–1.4 M), considering that high concentrated systems are relevant for industrial applications. This class of surfactants is also interesting as remediation agent since they can incorporate different polluting molecules, both polar and nonpolar, such as volatile Organic Compounds (VOCs) and

* Corresponding authors.
E-mail addresses: sandra.ristori@unifi.it (S. Ristori), margarita.sanchez@cimav.edu.mx (M. Sanchez-Dominguez), federico.rossi2@unisi.it (F. Rossi).

https://doi.org/10.1016/j.colsurfa.2023.131799
Received 27 March 2023; Received in revised form 1 June 2023; Accepted 2 June 2023
Available online 3 June 2023
0927-7757/© 2023 Elsevier B.V. All rights reserved.

Dense Non Aqueous Phase liquids (DNAPLs). The rheological and transport properties of SYN solutions were investigated through diffusion coefficients and viscosity, while shape and size of self-assemblies were determined by Dynamic Light Scattering and by Small Angle Scattering of Neutrons (SANS) and X-rays (SAXS). Results show that SYN generally behaves as other nonionic surfactants in dilute solutions, but shows some peculiarity of aggregate packing at high concentration. We recently demonstrated the efficiency of the Synperonic™ family of surfactants in solubilising trichloroethylene (TCE), in particular above a critical concentration of 0.1 M, thus being a good candidate for remediation purposes. Here, the solubility of TCE was correlated with the number and the size of micelles at different surfactant concentrations. Our work helps filling a gap in the literature about technical grade surfactants with odd-number carbons, and the results can help in assessing the performances of Synperonic™ products for technical tasks.

1. Introduction

It is well known that ethoxylated surfactant hydration, and therefore packing parameter and micellar structure are dependent on temperature, since hydrogen bonds break as temperature increases. In the literature, there are scant data on the phase behaviour of nonionic surfactants belonging to the class of Synperonic™ [1,2], and, to the best of our knowledge, very limited data is present about Synperonic™ 91/5 (SYN), an ethoxylated alcohol with a short polyethylene oxide chain (EO = 5 units) and an aliphatic chain ranging from 9 to 11 carbon atoms, depending on the formulation of the product; available data includes liquid-liquid equilibria diagram reporting the cloud point at different surfactant concentrations (up to [SYN] = 50 % the experimental cloud point was found to be above 25 °C) [3]. More data are present about the phase behaviour of the pure surfactant having a 10 carbon-tail, where a single L isotropic phase was reported for a concentration of surfactant up to 50 % at 25 °C [4,5]. To fill the gap, in this paper, we extend the structural study of the commercial surfactant Synperonic™ 91/5 to investigate its phase behaviour in a broader range of concentrations. This investigation can help in assessing the performances of Synperonic™ surfactants for technical tasks.

Among the different applications, the use of surfactants to improve the solubility of organic contaminants has been intensely studied over the past years, especially for implementing remediation techniques [6,7]. However, not all surfactants can be used for this purpose because residual products of their degradation can be toxic and/or the amphiphile itself gives rise to environmental contamination [8,9]. In this respect, ethoxylated fatty alcohol surfactants with chemical structure of the type $CH_3(CH_2)_{i-1}(OCH_2CH_2)_jOH$ (C_iEO_j), possess good environmental compatibility due to their biodegradability [10,11] and have been employed in many important applications, especially in household detergents [8,12]. Ethoxylated fatty alcohols have also been used in soil and water remediation, especially those applications related to surfactant/co-solvent flushing for enhancing the solubility of organic compounds in Pump & Treat remediation techniques [13], with a special emphasis on chlorinated DNAPLs (Dense Non Aqueous Phase liquids), such as trichloroethylene (TCE) and tetrachloroethylene (PCE). For example, Pennell et al. tested commercial ethoxylated nonionic surfactants such as Witconol 2722 (an ethoxylated sorbitan ester), Tergitol NP-15 (Nonylphenol Ethoxylate) and Witconol SN-120 ($C_{10-12}EO_9$) with good results [14] and Diallo et al. [15] tested the solubility of TCE and PCE as a function of the Hydrophilic-Lipophilic Balance (HLB) value [16–18].

In the case of C_iEO_j surfactants it is well established that the thermal behaviour, and particularly the cloud temperature, depends on the molecular structure [19,20]. Therefore, commercial nonionics of this class, which usually present a distribution of polyoxyethylene chain lengths as a result of the synthetic process, may exhibit a more restricted liquid–liquid immiscibility region or a higher cloud temperature, that are favourable aspects in many practical applications [21].

In recent studies we tested a series of commercial C_9-C_{11} alcohol ethoxylated surfactants belonging to the low-impact, cost-effective and biodegradable Synperonic™ class, to enhance the solubility of TCE in aqueous solutions [22–25]. The rational of our work was to assess the best trade-off among structural properties, EO unit number and HLB of the surfactants to obtain the best TCE solubility. Interestingly, all the Synperonic™ family surfactants exhibited a threshold concentration below which the solubility of TCE did not markedly increase. For example, for Synperonic™ 91/5 (SYN) in the range 6.1×10^{-4} M – 0.1 M the solubility of the organic molecule increased only by a factor 2 with respect to pure water (e.g. [TCE] ~ 0.02 M at [SYN] ~ 0.001–0.1 M), whilst, starting from 0.1 M, solubility increased significantly with the concentration of SYN up to a factor 15 at [SYN] = 0.75 M at 20 °C (e.g. [TCE] ~ 0.111 M at [SYN] ~ 0.5 M and [TCE] ~ 0.145 M at [SYN] ~ 0.75 M). It was speculated that the change in the TCE solubility reflected a dramatic change in the aggregation state of the surfactant at 0.1 M. In the case of Synperonic™ 91/5, here chosen as representative molecule of the Synperonic™ 91/N family, a marked change of rheological properties, a minimum of the diffusion coefficient and, simultaneously, a 15 times increase of TCE solubility was found to occur in the proximity of 0.1 M. This concentration range, therefore, required high-resolution structural investigation. Small angle scattering (SAS) of neutrons and X-rays is a powerful tool for characterizing micellar aggregates [26–28] in a wide range of concentrations. Here these techniques were used to investigate at high resolution the structural details of the aggregates and to elucidate the key factors which determine the behaviour of the viscosity and the transport properties of SYN as a function of the surfactant concentration.

2. Experimental

2.1. Chemicals

The surfactant Synperonic™ 91/5 (technical grade, hereafter abbreviated as SYN) was provided by CRODA and used without further purification. SYN has molecular formula $C_{9\text{-}11}EO_5$, MW = 378.42 g/mol, HLB = 12.54 and CMC = 5.5×10^{-4} M. Stock solutions were prepared by using deionized water from reverse osmosis (Elga, model Option 3) having a resistivity higher than 1 MΩ cm. It was determined that the water content of the surfactant was 0.87 %, by using the Karl Fischer technique (according to AOAC 984.20 Official Method); this was carried out by an automated potentiometric titration (in triplicate against a blank) with iodine and sulfur dioxide following an extraction with anhydrous chloroform/methanol.

2.2. Viscosity measurements

Viscosity measurements of aqueous solutions were carried out using an AR G2 rheometer from TA Instruments in a SYN concentration range of 1×10^{-4} – 1 M, at 25 °C, using as geometry a standard cone of steel of 44 mm and 2° of truncation. The shear rate measurement sweep was in a range of 0.1–100.0 s^{-1} with a tolerance percentage of 5 %.

2.3. DLS

The aqueous solutions of the surfactants were analysed by Dynamic Light Scattering (DLS) using the Zetasizer nano ZS (Malvern) at 25 °C, at a scattering angle of 173°, in a SYN concentration range of 0.01–1 M.

The following data were used for DLS measurements: refractive index of the surfactant 1.419, refractive index of water 1.33, absorption of the samples at 633 nm A = 0.0, and the viscosity of water was 0.8872 cP. The automatic algorithm, which uses a combination of monomodal (cumulants), non-negative least squares (NNLS) and CONTIN algorithms was used for data analysis.

2.4. Diffusion coefficients: Taylor dispersion analysis

Diffusion coefficients of SYN in water were measured by means of the Taylor dispersion technique [29–35]. This technique is based on the diffusive spreading of a solute, with a delta distribution function, injected into a flowing stream containing the solute itself but with a slightly different concentration. If the flow shows a parabolic velocity profile, after an *elution* (dispersion) process, the delta function distribution ends up having a bell shape, which can be fitted by a combination of n Gaussian functions. The diffusion coefficients are calculated from the parameters of the Gaussian functions that fit the eluted peak. For further details see Supporting Information.

2.5. Small-Angle Neutron Scattering (SANS) experiments

SANS measurements were carried-out on D33 at the Institut Laue-Langevin (ILL), Grenoble, France. An incident wavelength of 6.0 Å was selected (relative fwhm 10 %), and two detector distances were used: 2.0 and 12.0 m, with front panels at 1.2 m. Samples were prepared in heavy water (^2H_2O or D_2O) (Eurisotop, 99.9 % D) to increase the contrast between solvent and the hydrogenated detergent and to decrease the incoherent background originating from ^1H, and poured in Hellma quartz 110-QS cuvettes of 1 mm pathway, placed in a thermalized sample-changer at 25.0 °C. Data were reduced using Lamp, with the scattering of H_2O 1 mm as flat field and subtracting the empty cell as background. Absolute scale was obtained independently for both configurations with the flux of the attenuated direct beam.

2.6. Small-angle X-rays scattering (SAXS) experiments

SAXS experiments were performed at ID02 beamline [36] at ESRF – The European synchrotron, Grenoble, France. The wavelength of the incident photons was $\lambda = 1$ Å and the sample detector distance was 0.8 m, resulting in a range of wave-vector q magnitude of 8×10^{-3} – 0.75 $Å^{-1}$, with $q = (\frac{4\pi}{\lambda})\sin\theta$, 2θ being the scattering angle. Samples were placed in quartz capillaries of 1.5 mm in diameter. The temperature was 24 °C. Samples of SYN were diluted in water, at eight different concentrations in the range of 4.5×10^{-3} – 1.35 M.

2.7. Small-Angle Scattering (SAS) data analysis

Small Angle Scattering techniques are able to detect spatial fluctuations of Scattering Length Densities (*SLD*) in the range 1–1000 nm. The scattering data can generally be split in two contributions: one originating from the shape, size, size distribution and repartition of material within one scatterer, called the normalized form factor $P(q)$ ($P(0) = 1$), and one corresponding to the distribution in space of the scatterers, called the structure factor $S(q)\left(\lim_{q\to\infty} S(q)\to 1\right)$. The measured intensity $I(q)$ is then the specific differential scattering cross-section per unit scattering angle $\frac{d\Sigma}{d\Omega}(q)$ smeared by the instrumental resolution: $I(q) = \int \frac{d\Sigma}{d\Omega}(q) res(q) dq$ which is considered as Gaussian, and is neglected for SAXS (high resolution). The resolution was accounted for when modelling SANS data; in the following, $I(q)$ and $\frac{d\Sigma}{d\Omega}(q)$ are used interchangeably. The modelling is then done using the equation:

$$\frac{d\Sigma}{d\Omega}(q) = nV^2 \Delta SLD^2 P(q) S(q) + bkg \quad (1)$$

where n is the number density of scatterers of mean volume V and of average contrast ΔSLD, which is a difference of *SLD*. For X-rays, the *SLD* is proportional to the electronic density (and therefore insensitive to isotopes). For Neutrons, the *SLD* is isotope-dependent. The estimated *SLD* for C_iE_j in water is represented in Fig. 1 to explain the comparative advantages of SANS and SAXS for this system.

In SANS, the hydrogenated aliphatic tails and headgroups have rather similar contrasts to the deuterated solvent, i.e. the technique is sensitive to the overall molecule and its self-assembled structures, which makes SANS ideal to determine overall micellar dimensions. In SAXS, the contrast between solvent and aliphatic chains is of opposite sign to the contrast between solvent and headgroup, with an overall contrast between solvent and surfactant (ΔSLD) that is close to 0. As a result, SAXS will be highly sensitive to local heterogeneities (core-shell structures) as well as interactions due to dense packing, but barely sensitive to the overall dimensions of the assemblies of surfactants. For this reason, we explore first SANS data on a concentration range from 50 mM (2 %, relatively dilute) to 1 M (40 %, concentrated), and complete the analysis with SAXS data on concentrated samples (500–1350 mM, 20–50 %).

The SANS intensity profiles were analysed using sasfit [37]. The SAXS intensity profiles were analysed by the GENFIT software [38,39]. With both programs, the fitting parameters are obtained by minimizing χ^2 based on experimental uncertainties (obtained from Poisson statistics on the number of events). For further details on analysis see Supporting Information.

3. Results and discussion

With the aim of understanding the behaviour of SYN in the surrounding of the threshold value 0.1 M, a series of physico-chemical analysis were performed in the range 1×10^{-4} M < [SYN] < 1.35 M, including diffusivities of SYN molecules, viscosity and structural investigations by means of DLS and X-rays scattering.

3.1. Physico-chemical characterization

Shear viscosity was measured for SYN solutions in the range 1×10^{-4} M < [SYN] < 1 M and results are reported in Fig. 2 (numerical values are reported in Table S3 of the SI). Viscosity is rather low and almost constant up to [SYN] = 0.1 M but it increases sharply above this threshold concentration (Fig. 2a). This may indicate a change in the

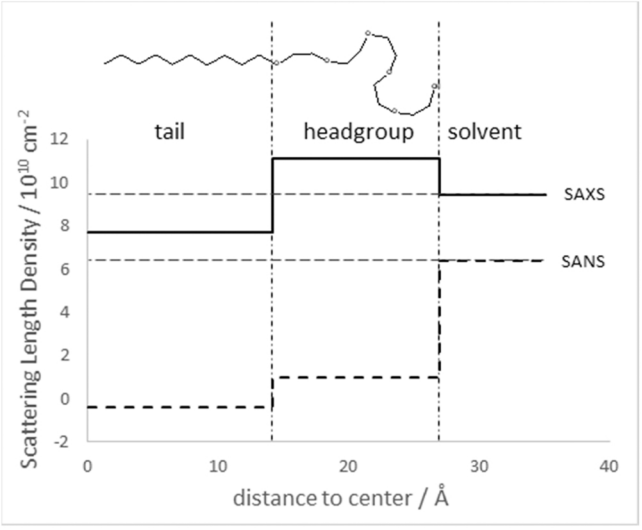

Fig. 1. Scattering length density profiles for X-rays and neutrons of the aliphatic chain, headgroup and solvent.

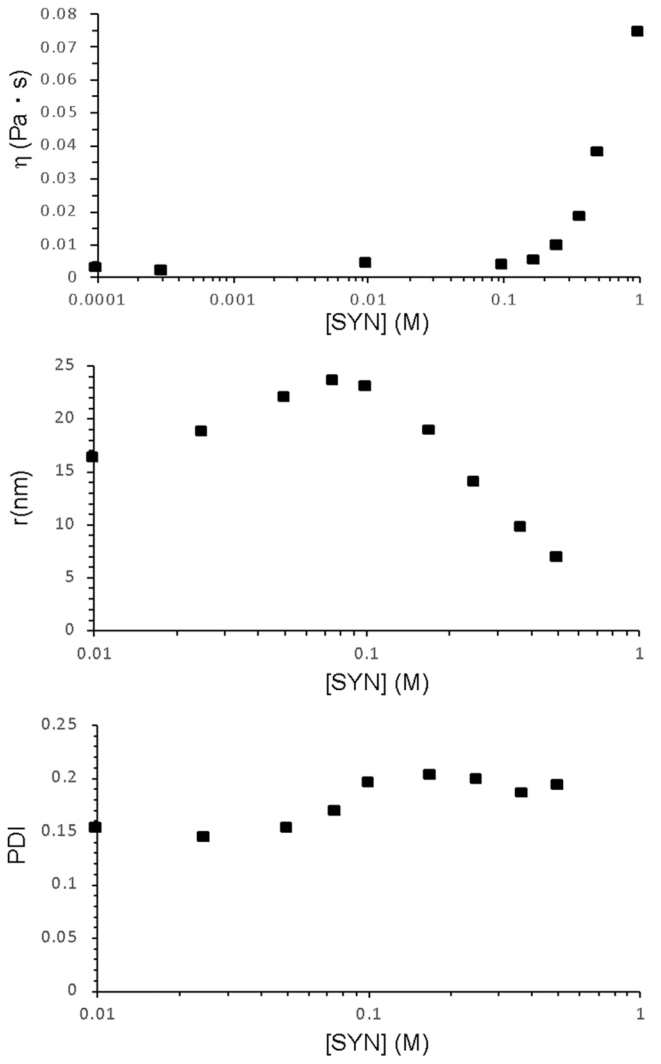

Fig. 2. Shear viscosity (η), hydrodynamic radius (*r*) and polydispersity index (PDI) as a function of surfactant concentration at T = 25 °C.

morphology of the micelles. It is well known that the viscosity of micellar solutions is directly related to their microstructure. The viscosity increases with the rise of concentrations of surfactant and other parameters, such as added salt or other additives [40]. Micelles can adopt various shapes such as spheres, elongated ellipsoids, cylinders (rods) and disks/bilayers; the longer rod-like flexible micelles are also known as wormlike micelles. Indeed, with the nonionic surfactant $C_{12}E_5$ at a concentration of 0.5 wt% ~200 times higher than the CMC (0.0029 wt%), Talmon et al. [41] observed the coexistence of spheroidal and elongated, threadlike micelles by Cryo-TEM. Imanishi and Einaga characterized polymer-like micelles formed with pentaoxyethylene decyl $C_{10}E_5$ and hexaoxyethylene decyl $C_{10}E_6$ ethers in dilute aqueous solution by SLS and DLS measurements [42]. The SLS data were analysed using the wormlike spherocylinder model. It was found that the micelles grow in size with increasing concentration and temperature, in conformity with the theoretical prediction for highly extended polymer-like micelles. Such studies were carried out with high purity C_iE_j surfactants with monodisperse EO chain and even numbered hydrocarbon chain, unlike our study, in which technical grade surfactants were used, which comprise a mixture of chain lengths, in particular for the ethylene oxide chain, plus a mixture of odd numbered hydrocarbon chain (C9–C11). The use of such type of commercial non-ionic surfactants is a requirement in our study due to the potential application, since this will reduce the cost significantly. However, the aforementioned works give an insight into the possible self-assembled structures formed by the Synperonic™ 91 surfactant series.

As for the hydrodynamic radius, DLS measurements were only possible above 0.01 M when the counts number started to be significant to obtain reliable data. In the range 0.01–0.075 M the aggregates radius increased linearly (Fig. 2b and Table S4 in SI), with a low polydispersity (Fig. 2c), until a plateau ($r \sim 23$ nm) was attained at [SYN] = 0.075 M. In the proximity of 0.1 M and above, the polydispersity increased significantly indicating the formation of different aggregates which structure could not be characterized properly by means of DLS.

Both the viscosity and the DLS measurements suggested [SYN] ~ 0.1 M as a threshold concentration where the SYN aggregates undergo a structural transition.

3.2. Diffusion coefficients

As an example of Taylor dispersion analysis, Fig. 3a reports the Taylor dispersion peaks obtained for three different injections of SYN in a flowing solution of [SYN] = 0.1 M in water at 25 °C. Squares, circles and triangles represent the experimental data for samples having an excess of surfactant of Δ[SYN] = 2.5, 5.0 and 7.5 × 10^{-2} M, respectively. Solid lines represent the best simulations of the experimental peaks obtained by simultaneously fitting the three experimental series with the equation (S1) in the SI, keeping *D* as shared parameter. The repetition of the fitting procedure for all the [SYN] explored, permitted to measure the diffusivities of the surfactant at different concentrations, as reported in Fig. 3b.

The trend of the diffusion coefficients with respect to the concentration of the surfactant clearly shows a minimum at [SYN] = 0.1 M where $D \sim 2.5 \times 10^{-7}$ cm^2/s. In the investigated range, the system is always above the CMC, therefore, in the range 0.001 – 0.1 M, diffusivities are referred to micelles, which grow with the addition of the surfactant to the system. When the concentration of SYN is augmented over 0.1 M, *D* increases up to $\sim 1 \times 10^{-6}$ cm^2/s when [SYN] = 1 M. This behaviour is quite common in solutions of nonionic surfactants when the system is in the proximity of a phase separation or a change in the structure of aggregates [43–45]. In the case of SYN, phase separation could be excluded since the solutions in the investigated range always appeared clear and without any evidence of macroscopic demixing. The

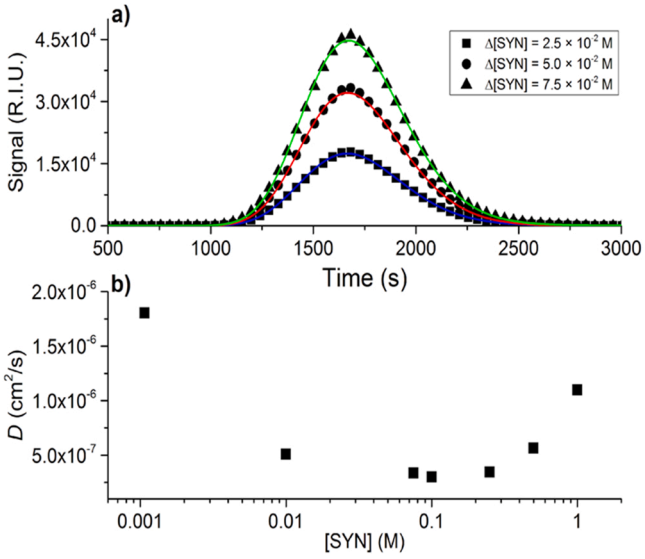

Fig. 3. a) Taylor dispersion peaks obtained by injecting samples having Δ[SYN] = 2.5 × 10^{-2} M (■), 5.0 × 10^{-2} M (●) and 7.5 × 10^{-2} M (▲), in a flowing solution with [SYN] = 0.1 M. Solid lines are the best fitting curves obtained by means of equation (S1) in the SI; b) Diffusion coefficient of SYN as a function of the concentration of the surfactant.

presence of a major transition in the aggregation state of the surfactant has emerged also from viscosity and laser scattering data, and the behaviour of D can be interpreted by considering an analogy with diluted polymeric systems [45,46], which is particularly suited to describe surfactants organising in 1-dimensional growing aggregates. When the concentration of the surfactant overcomes a certain threshold, a transition takes place from the individual diffusion of micelles to the collective motion of entangled networks of surfactant aggregates. In the framework of the Taylor dispersion analysis, the presence of such structured network would improve the radial diffusion of the molecules that render the sample less dispersed in the axial direction of the flow, thus resulting in a higher diffusion coefficient.

3.3. SAS analysis

Small Angle Neutron Scattering (SANS) profiles are presented in Fig. 4 with their modelling. At 50 and 100 mM (2 % and 4 %), the intensity profiles follow closely q^{-1}, which is the signature for elongated 1D structures. Data modelling was performed with wormlike micelles, i.e. flexible cylinders; the model takes into account the overall flexible rod behaviour according to Kholodenko [47], while the scattering from the circular cross-section is concentric, core-shell, with a polymer-like contribution from the solvated polar headgroup as suggested by Svaneborg and Pedersen [48]. The fitting parameters are given in Table 1. The aggregation number (mean number of surfactant per micelle) is around 1000 and decreases from 50 to 100 mM. At 500 and 1000 mM (20 % and 40 %), intensity profiles are dominated by a peak, originating from the correlation between scatterers due to dense packing. The mean center-of-mass distance between neighbours can then be approximated by $D^* = 2\pi/q_{peak}$, which gives 101 and 63 Å respectively for 20 % and 50 %. Concentrated wormlikes do not exhibit a peak but a flattening of the intensity [49,50]. Such a peak is instead characteristic of spheroidal scatterers interacting with their neighbours in 3 dimensions, or of lamellae stacks in one dimension (perpendicular to the lamellae). In both cases, a second peak is expected at twice the q-value of the first peak (exactly for a perfect stack of lamellae, while 2 is only an approximation for spheroidal interactions). SANS data show no obvious

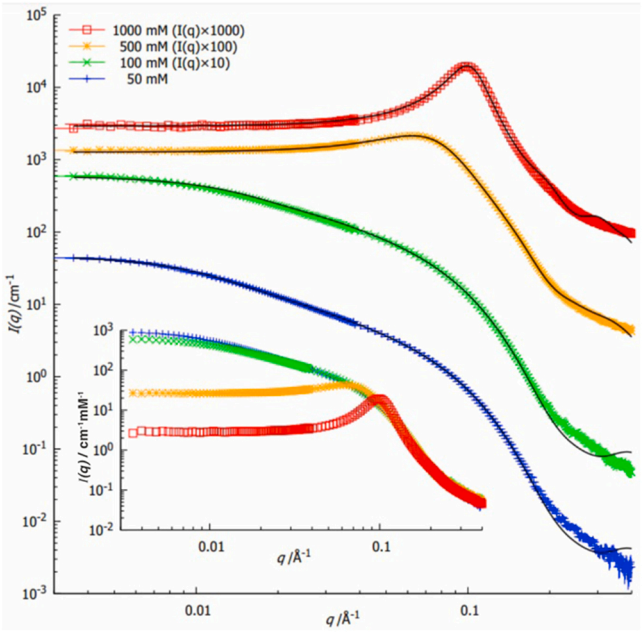

Fig. 4. SANS intensity profiles from SYN solutions in D_2O at 50, 100, 500 and 1000 mM, with their modelling (continuous black lines). Incoherent background (as determined from the fit) has been subtracted from the experimental profiles. Inset shows data in absolute scale, normalized by concentration.

Table 1
Fit parameters for the SANS intensity profiles displayed in Fig. 4. At 100 mM, the model for wormlike gives a persistence length larger than the contour length, i.e. the cylindrical micelles are rigid.

Fit with wormlikes			Fit with interacting disks		
	50 mM	100 mM		500 mM	1000 mM
number density/μm^3	2.5·10^4	9.2·10^4	number density/μm^3	1.5·10^6	9.4·10^6
aggregation number	1157	671	aggregation number	76	31
core radius/Å	13.8	13.8	core thickness/Å	13.4	15.0
Gyration radius headgroup/Å	6.4	6.4	Gyration radius headgroup/Å	6.4	6.4
Contour length/Å	576	334	core radius/Å	23.1	14.0
Persistence length/Å	333	*(rod)	Excluded volume fraction	17 %	36 %

evidence for such a peak; SAXS data however display this second peak for the highest concentrations explored (1.15 M and 1.35 M), see Fig. 6. The main peak position obtained from SANS and SAXS is the same as that obtained on monodisperse $C_{10}EO_5$ by Degiorgio et al. at 35 °C, i.e. above liquid crystalline regions [51], as shown in Fig. 5. The linear variation of q_{peak} with the volume fraction corresponds to what is expected for a one-dimensional dilution law, as typical for lamellae. SYN and the monodisperse $C_{10}EO_5$ seem to behave similarly. SANS data for 500 and 1000 mM were modelled with spheres, ellipsoids, rods and disks [52], modified according to [48] and the latter were found to describe better the data, the corresponding modelling is displayed in Fig. 4 (black solid lines). All models indicated the same behaviour in any case: the aggregation number is close to 100, i.e. one order of magnitude less than at 50 – 100 mM, and decreases between 500 and 1000 mM. The micelles are now close to be isotropic, i.e. the one-dimensional elongation observed at lower concentration is entirely lost. A hard sphere structure factor is used in our fits. The main parameters obtained from fits of the SANS data, given in Table 1, show the following:

(1) the aggregation number decreases steadily with concentration, almost as its reciprocal (N_{agg}~60000/[SYN]), (2) consequently the number density of micelles increases quicker than the concentration (almost quadratically): micelle/μm^3 ~$8 \times 10^6 \times$ [SYN]^2, (3) the drastic reduction of aggregation number correlates with a continuous change from long flexible cylinders to rigid cylinders to small, almost spheroidal disks and (4) the aliphatic chains determine the core dimension at about 14 Å. The fact that almost spheroidal aggregates are observed at 1 M

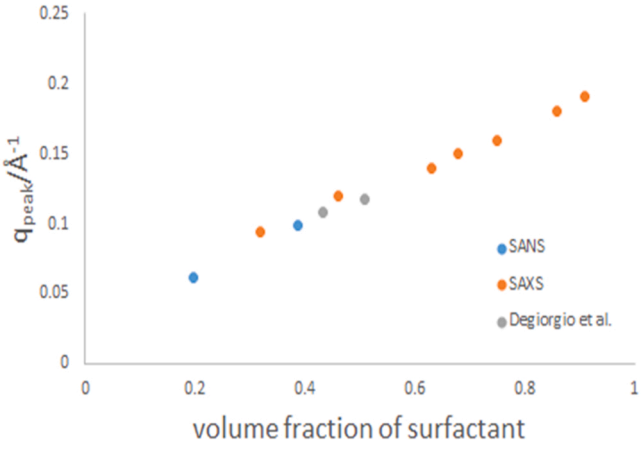

Fig. 5. Peak position from SANS and SAXS data compared to those obtained on pure monodisperse $C_{10}EO_5$ by SANS [51]. The linear variation of q_{peak} follows a one-dimensional dilution law.

seems to be contradictory to the linear dilution law for the peak obtained at and above 0.5 M, but is in line with the conclusion of Degiorgio that with increasing concentration "*the micellar structure becomes less and less sharp, but some orientational correlations between neighboring amphiphile molecules still exist*". The description of data with well-defined core-shell micelles becomes less relevant, and the main interaction between nearest neighbours is mostly one-dimensional but short range (i.e. disorder prevents long-range alignment as seen in liquid crystalline phases), which is why a hard sphere structure factor for liquids reproduces the SANS data reasonably well.

Small Angle X-ray Scattering (SAXS) profiles are shown in Fig. 6, together with their best fits obtained with the Modified Scattering Density Profile model (MSDP, see supporting information for details). The quality of the fits in the whole range of q can be easily appreciated, indicating, in general, that the adopted model of infinite flat bilayers is able to describe the structure of SYN samples in all the investigated concentrations. Data have been also analysed with other micellar models, including spheres, spherocylinders and bicelles, with and without interaction, but fitting results, here not reported, were very poor, suggesting that the technical grade SYN samples show a different structural behaviour with respect to the pure ethoxylated alcohols [40, 45,53]. On the contrary, the MSDP model seems to be able to catch the average features of the mixture of molecules contained in the SYN samples, which result to be mostly organized in sheets, with diverse levels of vertical correlation as a function of SYN concentration.

The common fitting parameters obtained by the MSDP analysis are reported in Table 2. The most significant single curve parameters are

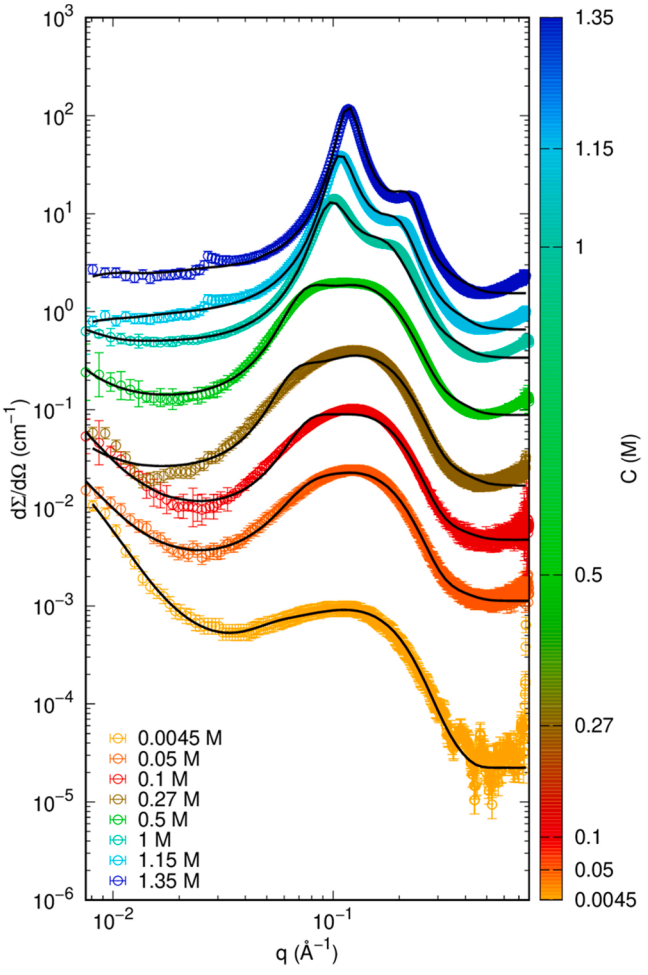

Fig. 6. SAXS experimental curves (symbols) and best fits (black line) of SYN solutions in water.

Table 2
Common fitting parameters.

m	ν_{CH_2} / Å^3	r_{13}	ν_{pol} / Å^3	d_h	ν_{wat} / Å^3
10.5 ± 0.2	26.91 ± 0.02	1.83 ± 0.01	337.0 ± 0.4	1.013 ± 0.002	29.20 ± 0.02

reported, as a function of SYN concentration, in the panels of Fig. 7. For the sake of completeness, the numerical values of all curves fitting parameters are listed in Tables S5 and S6 of the Supporting Material.

The average number m of CH_2 groups in the hydrophobic chain is found to be 10.5 ± 0.2, close to the maximum value stated by the technical sheet of SYN. All the other common fitting parameters assume values in very good agreement with published results [54–56], including the mass density of hydration water, which has been found to be ~1 % higher than the bulk water density. By looking to the overall trends of the single curve fitting parameters, reported in Fig. 7, it can be clearly noticed that there is a marked change (evidenced by a vertical grey stripe) at SYN concentration close to 0.1 M, which is in very good agreement with the results obtained by DLS, shear viscosity and diffusivity measurements. More in details, the area per molecule changes from ~62 Å^2 at 0.0045 M to a much higher value close to 75 Å^2 at the highest concentrations. This effect is a combination of the reduction of the hydrophobic length D_{hyd} that decreases, as a function of SYN concentration, from ~5.5 Å to ~4.2 Å, whereas the length of the polar head, *2w_pol*, increases from ~14 Å to ~16 Å. This result suggests possible variations, driven by the SYN concentration, of conformation or hydration properties of the ethoxylated polar heads. Indeed, the number of hydration water molecules *per* polar head (Fig. 7), simply derived by the fitting parameters, markedly changes from ~35 to ~55. The phenomenon can be better understood by observing the volume fraction distributions of the different groups reported in Fig. 8. The most relevant difference among the curves occurs at SYN concentration ~0.1 M. In particular, the changes involve the volume fraction distribution of the hydration water (dotted lines) and the one of the polar group (dashed lines).

The parameters c, N and g_c (Fig. 7) that describe the para-crystal staking among bilayer show a trend with SYN concentration more

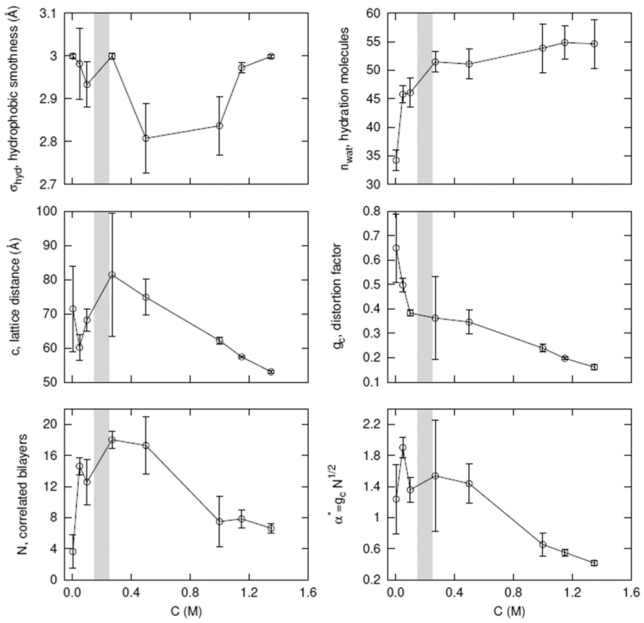

Fig. 7. Single fitting parameters obtained by the analysis of SAXS data with the MSDP model. The grey stripe indicates the concentration region at which a transition is observed by different techniques used in this work (see text for more details).

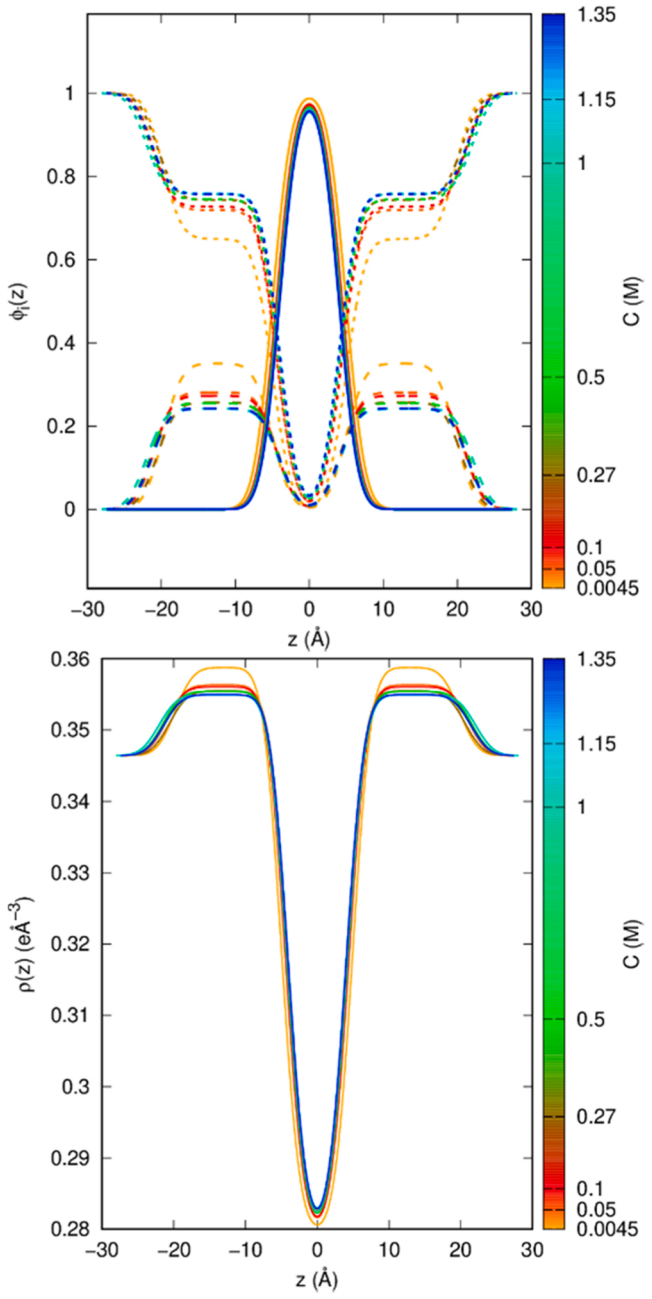

Fig. 8. Top panel: volume fraction distribution as a function of the distance z from the bilayer mid-plane of the hydrophobic group (solid lines), the polar head group (dashed lines) and the hydration water group (dotted lines) obtained by the analysis of SAXS data with the MSDP model. Colours refer to SYN concentrations according to the key of Fig. 3. Bottom panel: electron density profiles calculated with Eq. 1.

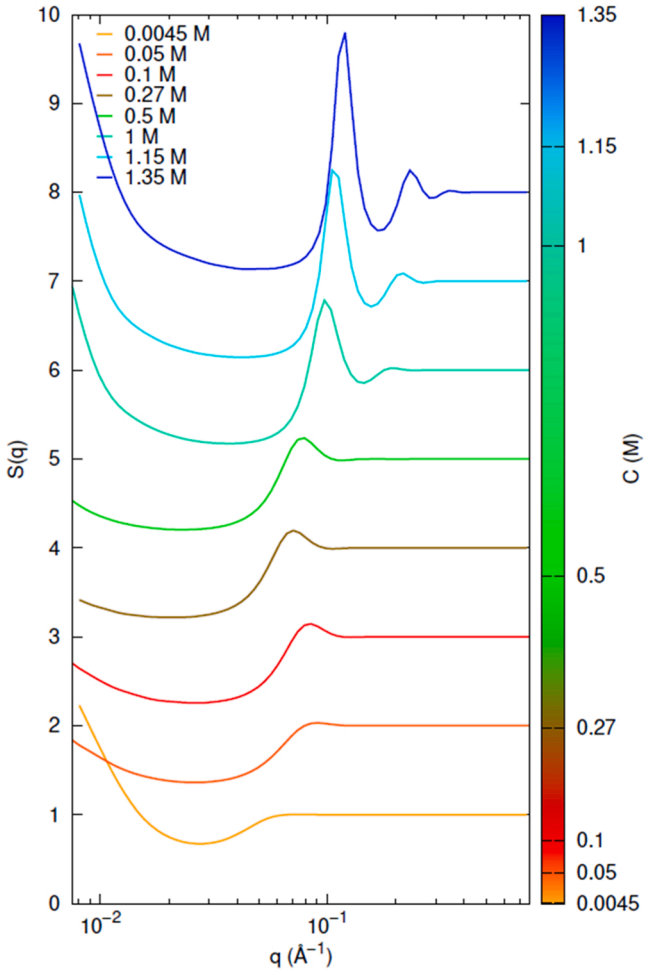

Fig. 9. Structure factors obtained by the fit of SAXS data of SYN samples with the MSDP model.

difficult to rationalize. At concentration ~0.1 M, the number of correlated lamellae is small, but the distortion parameter is so high that the fitted values of the lattice distance *c* can be considered meaningless. On the other hand, different parameters extracted from the fit of SAXS diagrams can account for the increased correlation and the narrowing of the observed quasi-Bragg peaks at very high SYN concentration, namely the enhanced intensity of the structure factor shown in Fig. 9 and the product $g_c \cdot N^{1/2}$, whose trend is reported in the bottom right panel of Fig. 7. This product is indicated as α * in the para-crystal theory and its value decreases with increasing correlation among bilayers [57,58].

More in detail, the profiles of the calculated structure factor as a function of concentration (Fig. 9) show that inter-aggregate correlations at the nanoscale are practically absent below 0.1 M, while moderate interactions appear in the proximity of 0.1 M and steadily increase above this threshold. Noteworthy, as mentioned above, this is the same surfactant concentration at which the viscosity and diffusion coefficients show marked change (see Figs. 2 and 3), indicating that the structure factor is closely related to the motion of SYN aggregates and that it can be responsible for the observed change of diffusive regime in solution. In this light, SAS results provide a refinement to the data obtained by techniques which report on the behaviour of bulk system.

4. Conclusions

In this work, we performed an in depth physico-chemical analysis of Synperonic™ 91/5 self-assembly behaviour. In particular, we focused in the concentration range around 0.1 M to correlate the microstructure with the performance efficiency of the surfactant as a solubility-enhancer for chlorinated solvents. All the techniques employed and the measured parameters (viscosity, hydrodynamic radius and diffusion coefficient) indicated a critical concentration threshold ($[SYN]_{cr}$ ~ 0.1 M) above which larger or more strongly interacting aggregates form in the aqueous medium. SAXS and SANS were then used as structural techniques, confirming the presence of $[SYN]_{cr}$ at which correlation among aggregates starts. They also allowed to identify the structure factor, reflecting the inter-micelle arrangement, as the key parameter for the transition between different diffusive regimes. The overall picture given by SAS investigation is that aqueous solutions of Synperonic™ 91/5 form elongated micelles up to 0.1 M, while at higher concentration a

marked reduction of size occurs and the shape of single scatterers evolves toward flat aggregates. We can thus represent the SYN micelles as flexible cylinders, virtually not interacting up to 0.1 M and as arrays of correlated, highly hydrated, lamellae in more concentrated systems. This evolution of shape and correlation is well in line with the phase diagrams reported in the literature for the C_iEO_j surfactant series and for $C_{10}EO_5$ in particular [5] and may help to specify the nanostructure of the lamellar (L) region found by Nibu et al. through DSC and FTIR [5]. These findings are important to shed light on our previous studies, which pointed out a dramatic change, at [SYN] = 0.1 M, in the solubility of TCE [22,23] and in the mass transfer rate from a pool of pure TCE to the bulk of surfactant solutions [24]. In fact, the transition from long cylinders to small discs implies an increase in the number of micelles and larger area per head groups. In conclusion, we showed how a detailed understanding of self-assembled microstructures can guide the optimization of applications. In our case, [SYN] = 0.1 M turned out to be a critical concentration starting from which the solubility and mass transfer of the organic molecule drastically increased with the concentration of the surfactant.

Electronic Supplementary Information

Electronic Supplementary Information (ESI) available: Experimental and computational details; Viscosity and DLS measurements. See DOI: 10.1039/x0xx00000x.

CRediT authorship contribution statement

Sara Falsini: Investigation, Formal analysis, Writing – review & editing. **Adriano Intiso**: Investigation. **Francesco Spinozzi:** Methodology, Formal analysis, Software, Writing – original draft, Writing – review & editing. **Sandra Ristori:** Investigation, Writing – original draft, Writing – review & editing, Supervision. **Nadia Marchettini:** Writing – original draft, Supervision. **Javier I. Garza-Arévalo:** Investigation. **Sylvain Prevost:** Investigation, Methodology, Formal analysis, Software, Writing – review & editing. **Margarita Sanchez-Dominguez:** Conceptualization, Methodology, Investigation, Writing – original draft, Writing – review & editing, Supervision. **Federico Rossi:** Conceptualization, Methodology, Investigation, Writing – original draft, Writing – review & editing, Supervision.

Declaration of Competing Interest

The authors declare that they have no known competing financial interests or personal relationships that could have appeared to influence the work reported in this paper.

Data Availability

Data will be made available on request.

Acknowledgements

We thank the large-scale facilities ESRF - The European Synchrotron and the Institut Laue-Langevin (ILL), Grenoble, France, for beamtime allocation at the ID02 and D33 instruments respectively. Analysis and assistance for DLS (Lilia Bautista, CIMAV S.C. Unidad Monterrey) and viscosity measurements (Patricia Cerda, CIMAV S.C. Unidad Monterrey) are acknowledged.

Appendix A. Supporting information

Supplementary data associated with this article can be found in the online version at doi:10.1016/j.colsurfa.2023.131799.

References

[1] C. Aubery, C. Solans, M. Sanchez-Dominguez, Tuning high aqueous phase uptake in nonionic water-in-oil microemulsions for the synthesis of Mn–Zn ferrite nanoparticles: phase behavior, characterization, and nanoparticle synthesis, Langmuir 27 (2011) 14005–14013, https://doi.org/10.1021/la203125x.
[2] C. Aubery, C. Solans, S. Prevost, M. Gradzielski, M. Sanchez-Dominguez, Microemulsions as reaction media for the synthesis of mixed oxide nanoparticles: relationships between microemulsion structure, reactivity, and nanoparticle characteristics, Langmuir 29 (2013) 1779–1789, https://doi.org/10.1021/la303817w.
[3] R.R. Racheva, Development of a Surfactant-based in Situ Extraction from Authentic Feedstocks, Thesis, Technische Universität Hamburg, 2020, https://doi.org/10.15480/882.2555.
[4] J.C. Lang, R.D. Morgan, Nonionic surfactant mixtures. I. Phase equilibria in C10E4–H2O and closed-loop coexistence, J. Chem. Phys. 73 (1980) 5849–5861, https://doi.org/10.1063/1.440028.
[5] Y. Nibu, T. Inoue, Phase Behavior of Aqueous Mixtures of Some Polyethylene Glycol Decyl Ethers Revealed by DSC and FT-IR Measurements, J. Colloid Interface Sci. 205 (1998) 305–315, https://doi.org/10.1006/jcis.1998.5621.
[6] E.J. Acosta, S. Quraishi, Surfactant Technologies for Remediation of Oil Spills, in: P. Somasundaran, P. Patra, R.S. Farinato, K. Papadopoulos (Eds.), Oil Spill Remediation, John Wiley & Sons, Inc, 2014, pp. 317–358, https://doi.org/10.1002/9781118825662.ch15.
[7] X. Mao, R. Jiang, W. Xiao, J. Yu, Use of surfactants for the remediation of contaminated soils: a review, J. Hazard. Mater. 285 (2015) 419–435.
[8] N.T. de Oude, The Handbook of Environmental Chemistry: Anthropogenic Compounds - Detergents v. 3/F, Springer-Verlag Berlin and Heidelberg GmbH & Co. K, Berlin, 1992.
[9] Z. Mao, X.-F. Zheng, Y.-Q. Zhang, X.-X. Tao, Y. Li, W. Wang, Occurrence and biodegradation of nonylphenol in the environment, Int J. Mol. Sci. 13 (2012) 491–505, https://doi.org/10.3390/ijms13010491.
[10] M.J. Scott, M.N. Jones, The biodegradation of surfactants in the environment, Biochim. Et. Biophys. Acta (BBA) - Biomembr. 1508 (2000) 235–251, https://doi.org/10.1016/S0304-4157(00)00013-7.
[11] L. Kravetz, J.P. Salanitro, P.B. Dorn, K.F. Guin, Influence of hydrophobe type and extent of branching on environmental response factors of nonionic surfactants, J. Am. Oil Chem. Soc. 68 (1991) 610–618, https://doi.org/10.1007/BF02660164.
[12] E.J. Acosta, The HLD–NAC equation of state for microemulsions formulated with nonionic alcohol ethoxylate and alkylphenol ethoxylate surfactants, Colloids Surf. A: Physicochem. Eng. Asp. 320 (2008) 193–204, https://doi.org/10.1016/j.colsurfa.2008.01.049.
[13] M.A. Cowell, T.C.G. Kibbey, J.B. Zimmerman, K.F. Hayes, Partitioning of Ethoxylated Nonionic Surfactants in Water/NAPL Systems: Effects of Surfactant and NAPL Properties, Environ. Sci. Technol. 34 (2000) 1583–1588, https://doi.org/10.1021/es9908826.
[14] K.D. Pennell, A.M. Adinolfi, L.M. Abriola, M.S. Diallo, Solubilization of Dodecane, Tetrachloroethylene, and 1,2-Dichlorobenzene in Micellar Solutions of Ethoxylated Nonionic Surfactants, Environ. Sci. Technol. 31 (1997) 1382–1389, https://doi.org/10.1021/es960604w.
[15] M.S. Diallo, L.M. Abriola, W.J. Weber, Solubilization of Nonaqueous Phase Liquid Hydrocarbons in Micellar Solutions of Dodecyl Alcohol Ethoxylates, Environ. Sci. Technol. 28 (1994) 1829–1837, https://doi.org/10.1021/es00060a012.
[16] W.C. Griffin, Classification of Surface-Active Agents by HLB, J. Soc. Cosmet. Chem. 1 (1949) 311–326.
[17] W.C. Griffin, Calculation of HLB Values of Non-ionic Surfactants, J. Soc. Cosmet. Chem. 5 (1954) 249–256.
[18] J.T. Davies, A quantitative kinetic theory of emulsion type. I. Physical chemistry of the emulsifying agent, Gas. /Liq. Liq. /Liq. Interface Proc. Int. Congr. Surf. Act. (1957) 426–438.
[19] R. Zana, C. Weill, Effect of temperature on the aggregation behaviour of nonionic surfactants in aqueous solutions, J. Phyique Lett. 46 (1985) 953–960, https://doi.org/10.1051/jphyslet:019850046020095300.
[20] T. Inoue, H. Ohmura, D. Murata, Cloud point temperature of polyoxyethylene-type nonionic surfactants and their mixtures, J. Colloid Interface Sci. 258 (2003) 374–382, https://doi.org/10.1016/S0021-9797(02)00162-5.
[21] H.C. Kim, J.-D. Kim, The polydispersity effect of distributed oxyethylene chains on the cloud points of nonionic surfactants, J. Colloid Interface Sci. 352 (2010) 444–448, https://doi.org/10.1016/j.jcis.2010.08.078.
[22] A. Intiso, Y. Miele, N. Marchettini, A. Proto, M. Sánchez-Domínguez, F. Rossi, Enhanced solubility of trichloroethylene (TCE) by a poly-oxyethylene alcohol as green surfactant, Environ. Technol. Innov. 12 (2018) 72–79, https://doi.org/10.1016/j.eti.2018.08.001.
[23] J.I. Garza-Arévalo, A. Intiso, A. Proto, F. Rossi, M. Sanchez-Dominguez, Trichloroethylene Solubilization Using A Series Of Commercial Biodegradable Ethoxylated Fatty Alcohol Surfactants, J. Chem. Technol. Biotechnol. 94 (2019) 3523–3529, https://doi.org/10.1002/jctb.5965.
[24] N. Valletti, M.A. Budroni, I. Lagzi, N. Marchettini, M. Sanchez-Dominguez, F. Rossi, Interfacial Mass Transfer in Trichloroethylene/Surfactants/ Water Systems: Implications for Remediation Strategies, Reactions 2 (2021) 312–322, https://doi.org/10.3390/reactions2030020.
[25] N. Valletti, M.A. Budroni, P. Albanese, N. Marchettini, M. Sanchez-Dominguez, I. Lagzi, F. Rossi, Hydrodynamically-enhanced transfer of dense non-aqueous phase liquids into an aqueous reservoir, Water Res. 231 (2023), 119608, https://doi.org/10.1016/j.watres.2023.119608.

[26] C. David, F. Pignon, T. Narayanan, M. Sztucki, G. Gésan-Guiziou, A. Magnin, Spatial and Temporal in Situ Evolution of the Concentration Profile during Casein Micelle Ultrafiltration Probed by Small-Angle X-ray Scattering, Langmuir 24 (2008) 4523–4529, https://doi.org/10.1021/la703256s.
[27] S. Falsini, L. Ciani, A. Arcangeli, E. Di Cola, F. Spinozzi, S. Ristori, Physico-chemical properties of gemini micelles studied by X-ray scattering and ESR spectroscopy, Colloids Surf. A: Physicochem. Eng. Asp. 472 (2015) 101–108, https://doi.org/10.1016/j.colsurfa.2015.02.034.
[28] L.K. Shrestha, S.C. Sharma, T. Sato, O. Glatter, K. Aramaki, Small-angle X-ray scattering (SAXS) study on nonionic fluorinated micelles in aqueous system, J. Colloid Interface Sci. 316 (2007) 815–824, https://doi.org/10.1016/j.jcis.2007.08.005.
[29] A. Alizadeh, C.A. Nieto de Castro, W.A. Wakeham, The theory of the Taylor dispersion technique for liquid diffusivity measurements, Int. J. Thermophys. 1 (1980) 243–284, https://doi.org/10.1007/BF00517126.
[30] R. Callendar, D.G. Leaist, Diffusion coefficients for binary, ternary, and polydisperse solutions from peak-width analysis of taylor dispersion profiles, J. Solut. Chem. 35 (2006) 353–379.
[31] V.K. Vanag, F. Rossi, A. Cherkashin, I.R. Epstein, Cross-Diffusion in a Water-in-Oil Microemulsion Loaded with Malonic Acid or Ferroin. Taylor Dispersion Method for Four-Component Systems, J. Phys. Chem. B. 112 (2008) 9058–9070.
[32] F. Rossi, V.K. Vanag, E. Tiezzi, I.R. Epstein, Quaternary Cross-Diffusion in Water-in-Oil Microemulsions Loaded with a Component of the Belousov−Zhabotinsky Reaction, J. Phys. Chem. B 114 (2010) 8140–8146, https://doi.org/10.1021/jp102753b.
[33] F. Rossi, V.K. Vanag, I.R. Epstein, Pentanary Cross-Diffusion in Water-in-Oil Microemulsions Loaded with Two Components of the Belousov-Zhabotinsky Reaction, Chem. Eur. J. 17 (2011) 2138–2145, https://doi.org/10.1002/chem.201002069.
[34] L. Chen, D.G. Leaist, Multicomponent Taylor Dispersion Coefficients, J. Solut. Chem. 43 (2014) 2224–2237, https://doi.org/10.1007/s10953-014-0268-y.
[35] F. Rossi, R. Cucciniello, A. Intiso, A. Proto, O. Motta, N. Marchettini, Determination of the trichloroethylene diffusion coefficient in water, AIChE J. 61 (2015) 3511–3515, https://doi.org/10.1002/aic.14861.
[36] T. Narayanan, M. Sztucki, P. Van Vaerenbergh, J. Léonardon, J. Gorini, L. Claustre, F. Sever, J. Morse, P. Boesecke, A multipurpose instrument for time-resolved ultra-small-angle and coherent X-ray scattering, J. Appl. Cryst. 51 (2018) 1511–1524, https://doi.org/10.1107/S1600576718012748.
[37] I. Breßler, J. Kohlbrecher, A.F. Thünemann, SASfit: a tool for small-angle scattering data analysis using a library of analytical expressions, J. Appl. Cryst. 48 (2015) 1587–1598, https://doi.org/10.1107/S1600576715016544.
[38] F. Spinozzi, C. Ferrero, M.G. Ortore, A. De Maria Antolinos, P. Mariani, GENFIT: software for the analysis of small-angle X-ray and neutron scattering data of macromolecules in solution, J. Appl. Crystallogr 47 (2014) 1132–1139, https://doi.org/10.1107/S1600576714005147.
[39] R. De Rosa, F. Spinozzi, R. Itri, Hydroperoxide and carboxyl groups preferential location in oxidized biomembranes experimentally determined by small angle X-ray scattering: Implications in membrane structure, Biochim Biophys. Acta Biomembr. 2018 (1860) 2299–2307, https://doi.org/10.1016/j.bbamem.2018.05.011.
[40] K.D. Danov, P.A. Kralchevsky, S.D. Stoyanov, J.L. Cook, I.P. Stott, E.G. Pelan, Growth of wormlike micelles in nonionic surfactant solutions: quantitative theory vs. experiment, Adv. Colloid Interface Sci. 256 (2018) 1–22, https://doi.org/10.1016/j.cis.2018.05.006.
[41] A. Bernheim-Groswasser, E. Wachtel, Y. Talmon, Micellar growth, network formation, and criticality in aqueous solutions of the nonionic surfactant C12E5, Langmuir 16 (2000) 4131–4140, https://doi.org/10.1021/la991231q.
[42] K. Imanishi, Y. Einaga, Effects of hydrophilic chain length on the characteristics of the micelles of pentaoxyethylene n-Decyl C10E5 and hexaoxyethylene n-Decyl C10E6 ethers, J. Phys. Chem. B 109 (2005) 7574–7581, https://doi.org/10.1021/jp044226q.
[43] Brown Wyn, Rymden Roger, Static and dynamical properties of a nonionic surfactant (C12E6) in aqueous solution, J. Phys. Chem. 91 (1987) 3565–3571, https://doi.org/10.1021/j100297a020.
[44] H. Ning, R. Kita, H. Kriegs, J. Luettmer-Strathmann, S. Wiegand, Thermal diffusion behavior of nonionic surfactants in water, J. Phys. Chem. B 110 (2006) 10746–10756, https://doi.org/10.1021/jp0572986.
[45] H.G. Thomas, A. Lomakin, D. Blankschtein, G.B. Benedek, Growth of mixed nonionic micelles, Langmuir 13 (1997) 209–218, https://doi.org/10.1021/la9606613.
[46] T.R. Carale, D. Blankschtein, Theoretical and experimental determinations of the crossover from dilute to semidilute regimes of micellar solutions, J. Phys. Chem. 96 (1992) 459–467, https://doi.org/10.1021/j100180a084.
[47] A.L. Kholodenko, Persistence length and related conformational properties of semiflexible polymers from Dirac propagator, J. Chem. Phys. 96 (1992) 700–713, https://doi.org/10.1063/1.462455.
[48] C. Svaneborg, J.S. Pedersen, Form factors of block copolymer micelles with excluded-volume interactions of the corona chains determined by Monte Carlo simulations, Macromolecules 35 (2002) 1028–1037, https://doi.org/10.1021/ma011046v.
[49] V.M. Garamus, J.S. Pedersen, H. Kawasaki, H. Maeda, Scattering from polymerlike micelles of TDAO in salt/water solutions at semidilute concentrations, Langmuir 16 (2000) 6431–6437, https://doi.org/10.1021/la000085h.
[50] L. Arleth, M. Bergström, J.S. Pedersen, Small-angle neutron scattering study of the growth behavior, flexibility, and intermicellar interactions of wormlike SDS micelles in NaBr aqueous solutions, Langmuir 18 (2002) 5343–5353, https://doi.org/10.1021/la015693r.
[51] V. Degiorgio, M. Corti, R. Piazza, L. Cantú, A.R. Rennie, Small-angle neutron-scattering study of concentrated nonionic-amphiphile solutions, Colloid Polym. Sci. 269 (1991) 501–505, https://doi.org/10.1007/BF00655888.
[52] J.S. Pedersen, Form factors of block copolymer micelles with spherical, ellipsoidal and cylindrical cores, J. Appl. Crystallogr. 33 (2000) 637–640, https://doi.org/10.1107/S0021889899012248.
[53] D. Lof, M. Tomsic, O. Glatter, G. Fritz-Popovski, K. Schillén, Structural characterization of nonionic mixed micelles formed by C12EO6 surfactant and P123 triblock copolymer, J. Phys. Chem. B 113 (2009) 5478–5486, https://doi.org/10.1021/jp808442d.
[54] J.B. Klauda, N. Kučerka, B.R. Brooks, R.W. Pastor, J.F. Nagle, Simulation-based methods for interpreting x-ray data from lipid bilayers, Biophys. J. 90 (2006) 2796–2807, https://doi.org/10.1529/biophysj.105.075697.
[55] N. Kucerka, J.F. Nagle, J.N. Sachs, S.E. Feller, J. Pencer, A. Jackson, J. Katsaras, Lipid bilayer structure determined by the simultaneous analysis of neutron and x-ray scattering data, Biophys. J. 95 (2008) 2356–2367, https://doi.org/10.1529/biophysj.108.132662.
[56] N. Kucerka, M.-P. Nieh, J. Katsaras, Fluid phase lipid areas and bilayer thicknesses of commonly used phosphatidylcholines as a function of temperature, Biochim. Biophys. Acta 2011 (1808) 2761–2771, https://doi.org/10.1016/j.bbamem.2011.07.022.
[57] F.J. Baltá-Calleja, R. Hosemann, The limiting size of natural paracrystals, J. Appl. Crystallogr. 13 (1980) 521–523, https://doi.org/10.1107/S0021889880012708.
[58] T. Frühwirth, G. Fritz, N. Freiberger, O. Glatter, Structure and order in lamellar phases determined by small-angle scattering, J. Appl. Cryst. 37 (2004) 703–710, https://doi.org/10.1107/S0021889804012956.